Orientational Probing of Multilayer 2-Mercaptobenzoxazole through NEXAFS: An Experimental and Theoretical Study

V. Carravetta*

Istituto di Chimica Quantistica ed Energetica Molecolare, C.N.R., via Risorgimento 35, 56100 Pisa, Italy

G. Contini

Institute of Mineral Processing, C.N.R., Via Bolognola 7, 00138 Roma, Italy

O. Plashkevych and H. Ågren

Institute of Physics and Measurement Technology, Linköping University, S-58183, Linköping, Sweden

G. Polzonetti

Department of Physics E. Amaldi, University Roma Tre, via della Vasca Navale 84, 00146 Roma, Italy

Received: December 4, 1998; In Final Form: March 21, 1999

Near edge X-ray absorption fine structure (NEXAFS) spectra of 2-mercaptobenzoxazole have been investigated from experimental and theoretical points of view. The 2-mercaptobenzoxazole molecule presents an interesting case for NEXAFS, with its aromatic, benzene-like, fragment and its heteroatom-rich part, containing C, N, O, and S atoms. NEXAFS spectra of a 2-mercaptobenzoxazole multilayer on Pt(111) at the carbon, nitrogen, and oxygen K-edges and at the sulphur L-edge have been recorded at normal and grazing incidence angles of the photon beam with respect to the surface. The C, N, and O K-edge spectra exhibit angular dependence in the π^* resonance region, indicating a mean orientation of the molecules on the surface. The angle between the molecular plane and the surface has been found to be about 48°. The experimental data are discussed by comparison with static-exchange (STEX) ab initio calculations for the different edges. Good agreement is observed between experiment and theory, allowing for a detailed discussion and attribution of the various features observed. A vibrational progression at the C K-edge is also identified in the highly resolved experimental spectrum.

I. Introduction

Studies of NEXAFS (near edge X-ray absorption fine structure) spectra of organic molecules, both free and interacting with surfaces, form nowadays a well established topic in chemical physics science.[1] Investigation of the bonding to metal surfaces of molecules having a π electron system, with the π and σ manifolds well separated, has greatly benefited from spectroscopic studies using NEXAFS.[1,2] In particular, they have been useful for probing the type and strength of the surface bond and the orientation of benzene-ring-based adsorbates under different conditions of preparation.

The bonding of 2-mercaptobenzoxazole (C_7H_5NOS, in the following MBO) to metal surfaces has a particular importance from a practical point of view, because this chemical species is employed in the mineral processing as a collector agent in flotation, in anticorrosion coatings on metals, and in the analytical determination of metals as a chelating complexant. An accurate interpretation of the NEXAFS spectra for the free MBO molecule is a prerequisite for the analysis of the corresponding spectra obtained when MBO interacts with various surfaces. Apart from the technical applicability of the molecule, a NEXAFS study of MBO is interesting since four different atomic species, C, N, O, and S, are present, forming an aromatic fragment and a reactive heteroatom-rich part. Because of the high chemical selectivity of X-ray photoabsorption, the spectra of these four centers can give complementary information for bonding and orientation. This is true also from a theoretical point of view because MBO is an excellent test case for the simulation of the NEXAFS spectra of a medium size, unsymmetrical planar molecule containing various atoms of different type. Only recent technical improvements[3,4] in the simulation field have made ab initio calculations also possible for complex organic compounds such as π electron conjugated heterocycles with more than one ring.

This paper contains NEXAFS spectra for the C, N, and O K-edges and S L-edge of MBO obtained experimentally under high-resolution conditions and from theoretically photoabsorption cross sections computed ab initio with a full accounting of core hole effects. The direct static exchange technique,[3] a fully ab initio method thoroughly tested in various other contexts,[4] is here employed for a detailed assignment of the spectra. Some of the edges here considered have recently been studied experimentally by some of us[5] but with a lower experimental resolution. The new more resolved experimental spectra allow a better and complete comparison with theory and, moreover, some vibrational resolved contributions at the C K-edge are identified.

II. Experimental Section

NEXAFS spectra were taken at LURE (Orsay, France), at the Super-ACO storage ring on the SACEMOR experimental

10.1021/jp984608u CCC: $18.00
Published on Web 06/17/1999

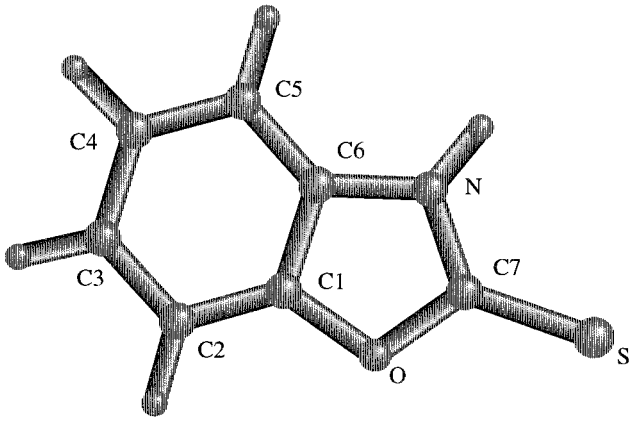

Figure 1. 2-Mercaptobenzoxazole (MBO) picture; the numbering of the seven carbon atoms is used in text.

station connected to the SA22 beam line at the bending magnet front end. The SACEMOR apparatus consists of three chambers isolable each other (background pressure is better than 5×10^{-9} Pa in all the chambers) including X-ray photoemission spectroscopy (XPS) and low-energy electron diffraction (LEED).

The Pt(111) single crystal (Material Research), was cleaned by argon ion sputtering with simultaneous heating at 900 K and annealing under vacuum. This procedure was checked using XPS, where no impurities were detected, LEED, where sharp (1×1) pattern was observed, and NEXAFS. The MBO sample has been supplied by Aldrich Chemical Company, Inc. Gas chromatography analysis gave purity of 98.4%. The main impurities were the crystallization solvents that have been removed before the dosing on the Pt(111) surface.

The structure of the MBO (thione form) is shown in Figure 1. MBO can exist also in the thiol tautomeric form (having the endocyclic double bond C═N and the hydrogen bonded to the sulphur atom); in the sample used in our experiment, only the thione form was present, as ascertained by XPS, infrared, and Raman measurements.

The MBO multilayer has been prepared in ultrahigh vacuum by evaporation (by heating to 115 °C), after repeated heating−pumping cycles, on a clean Pt(111) crystal. The inlet of the vapor from the sample holder to the chamber was controlled by means of a leak valve. To ascertain that at the temperature used no molecule decomposition occurs, infrared spectroscopy measurements on evaporated MBO have been carried out, showing no modification upon evaporation. The repeated heating-pumping cycles procedure has been effective in removing the impurities from the sample, as ascertained by infrared spectroscopy and gas chromatography. Before the dosing of the multilayer, the Pt(111) crystal was cooled down at 95 K using a liquid nitrogen cryostat.

The NEXAFS carbon, nitrogen, and oxygen K-edges and sulphur L-edges were recorded at two different incidence angles of the photon beam (ϑ) with respect to the Pt(111) surface, normal and grazing ($\vartheta = 15°$).

Signals from MBO (I_{MBO}) and from an evaporated gold grid (I_{grid}) were simultaneously recorded using respectively a channeltron collecting the partial secondary electron emission and a picoamperometer measuring the total current from the grid. The absorption signal is given by I_{MBO}/I_{grid}. The photon energy was calibrated at the carbon K-edge on the peak at 284.7 eV appearing in the absorption from the gold grid, due to weak contamination of the optics.

All the reported experimental spectra were normalized by fitting the part before absorption features by a straight line, taking it as zero, and assuming as unity the signal far beyond the σ^* resonances. The higher resolution π^* region of the C and N K-edges experimental spectra shown in the text have been normalized to the respective spectra recorded in a larger energy range.

Fittings of the π^* region of the experimental C and N K-edges have been obtained by the Levenburg-Marquardt nonlinear minimization algorithm using nonapproximated Voigt (Gaussian to Lorentzian deconvolution) functions. Unconstrained energy and widths (same Gaussian and Lorentzian widths for all the peaks) are used in the fits.

III. Computational Methods

The direct static exchange (STEX) method used in the present calculations has been described elsewhere[3] and applied to various different types of core electronic spectra.[4] In the STEX approach, a one-electron Hamiltonian containing a site specific (N-1) electron core potential is diagonalized for each ionization channel in order to obtain a photoabsorption spectrum of singly excited states. The potential for the excited electron is static with respect to the ion-electron interaction but the exchange interaction as well as the relaxation of the ion orbitals is fully accounted for.[3] The STEX Hamiltonian matrix is constructed directly from one- and two-electron integrals computed by adopting a double atomic orbital basis set algorithm.

The bound molecular orbitals (MO) are optimized by self-consistent field (SCF) calculations for the ground state and for each of the core-hole states (ΔSCF) and are expanded in a relatively small basis set, here Dunning basis set for C and N[6] (triple-ζ), and for H[6] (double-ζ plus polarizing), and by Sadlej for O[7] (triple ζ). Sulphur requires a good d function basis set to account for its coordination in the ground and excited states; a triple-d basis set is used in that case. For the calculation of the STEX Hamiltonian, augmentation of the basis sets with a large set of diffuse functions (20s, 18p, *2*0d) centered on the ionized site, has been employed. The geometry of the MBO molecule, see Figure 1, has been obtained from the Cambridge data base;[8] SCF optimization of MBO geometry produced spectra with only minor and negligible changes. Stieltjes imaging[9] is applied to the theoretical spectra to obtain the integrated photoabsorption cross section. The computed spectra are finally convoluted with a Gaussian function of different full width at half-maximum (fwhm) for the four calculated edges (exact values are given in the text) in order to simulate, roughly, the experimental resolution and the vibrational broadening that is not considered by the present calculations in the vertical transition approximation. In the following comparison of theoretical and experimental spectra, it should be kept in mind that the STEX spectra for low-lying valence-like levels appear in general pushed up in energy with respect to experiment, owing to errors because of the neglect of the electronic correlation and, mostly, because of the screening of the bound electrons with respect to the excited electron.

IV. Results and Discussion: Spectral Characterization

This section describes the comparison between the experimental and theoretical NEXAFS spectra of MBO.

The experimental spectra have been obtained for MBO adsorbed as a multilayer on a Pt(111) single crystal, whereas the calculations have been performed for the free isolated molecule. Free molecules may be considered a reasonable approximation for a multi-layer system, where the intermolecular forces are sufficiently weak to introduce only a minor perturbation in the electronic structure. The validity of such an

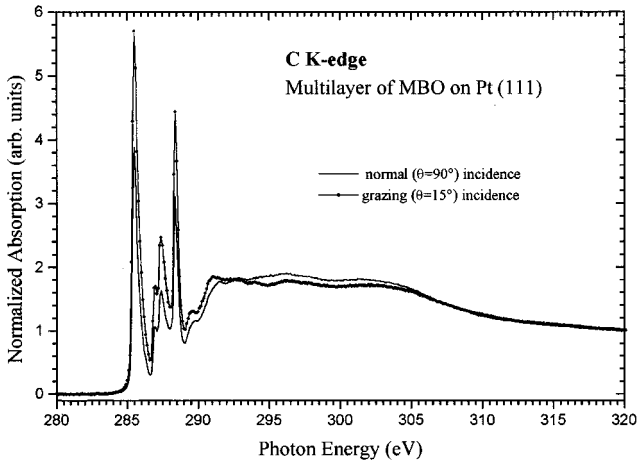

Figure 2. Experimental C K-edge spectra of MBO multilayer adsorbed on Pt(111) single crystal at 95 K, at grazing and normal photon incidence angle with respect to the surface.

TABLE 1: NEXAFS Experimental Energy Positions in the C, N, and O K-Edges and S L-Edge Spectra of MBO Multilayer[a]

C K-edge	N K-edge	O K-edge	S L-edge
285.5 (0)	402.8 (0)	536.4 (0)	159.1 (0)
287.0 (1.5)	404.3 (1.5)	537.8 (1.4)	160.7 (1.6)
287.4 (1.9)	408.2 (5.4)	540.7 (4.3)	161.7 (2.6)
288.4 (2.9)	412.2 (9.4)	546.2 (9.8)	162.8 (3.7)
289.6 (4.1)	406.1 IP	539.7 IP	164.0 (4.9)
291.1 (5.6)			169.5 (10.4)
296.2 (10.7)			174.6 (15.5)
302.5 (17.0)			167.9 IP
290.3 IP			
291.6 IP			
293.8 IP			

[a] The energy relative to the lowest value is shown in parentheses. Ionization thresholds (IP) from X-ray photoemission spectroscopy are reported in ref 23.

assumption is confirmed a posteriori by the good comparison of theoretical and experimental results in the following.

C, N, and O K-edges and S L-edge spectra will be discussed separately in the following subsections. STEX calculations at the C K-edge have been performed separately for each one of the seven inequivalent carbon atoms. The orientation of the MBO molecules with respect to the Pt surface is derived from the observed angular dependence of the experimental NEXAFS spectra at the three different K-edges in section IV.E.

A. Carbon K-Edge. The experimental C K-edge spectra recorded for the MBO multilayer on the Pt(111) surface (at 95 K) at grazing and normal incidence are reported in Figure 2. These spectra show a four-band structure between 285 and 290 eV (clearly identifiable at 285.5, 287.0, 287.4, and 288.4 eV) and comparatively weaker transitions at higher energy (found at 289.6, 291.1, 296.2, and 302.5 eV) (see Table 1).

Figure 3 collects the C K-edge spectra computed by the STEX method and convoluted with a Gaussian function (fwhm = 0.40 eV) for the seven inequivalent carbon atoms of MBO (from C_1 to C_7 in Figure 1) and the sum of these spectra (C_{tot}). Table 2 reports the theoretical main excitations with oscillator strengths and ionization thresholds for the seven carbon atoms.

The C_{tot} spectrum in Figure 3 can be compared with the experimental one reported in Figure 2; a more detailed comparison of the main spectral features can be made considering only the π^* region for which the total C K-edge (C_{tot}) spectrum is reported in Figure 4.

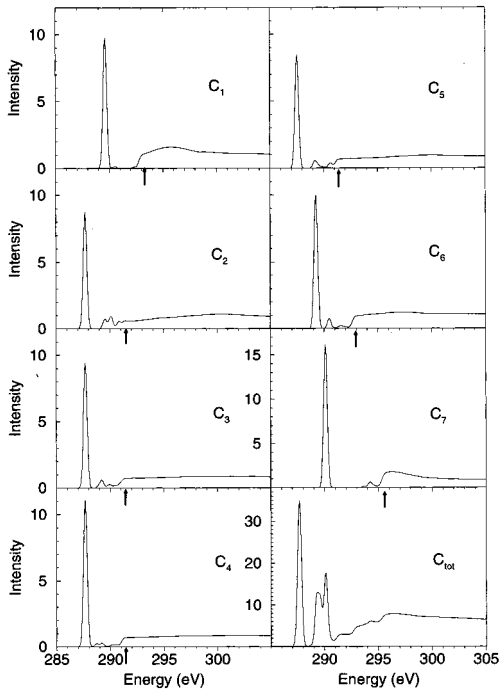

Figure 3. C K-edge spectra calculated by the STEX method for the seven inequivalent carbon atoms (C_1 to C_7) of MBO, convoluted with a Gaussian function (fwhm = 0.40 eV) in the low energy region. The sum of the C_1 to C_7 C K-edge spectra is indicated as C_{tot}. Arrows mark the positions of the core ionization thresholds.

From the ab initio simulations the four transitions appearing in the low energy region of the experimental spectrum, labeled from "a" to "d" in Figure 5, can be assigned to π^* resonances due to various inequivalent carbon atoms of the molecule (chemically shifted carbons). Carbon atoms C_2, C_3, C_4, and C_5 give rise to resonances close to each other that, as a sum, produce transition "a", while the carbon atoms C_6, C_1, and C_7 give the resonances "b", "c", and "d", respectively. Except for the energy shift previously discussed, we find a good agreement between experimental and calculated spectra.

The strong 285.5 eV feature in Figure 5 is typical for benzene carbons that are unconnected to any substituent (C_2, C_3, C_4, and C_5). This feature seems inert to any environmental change and serves as an excellent spectral fingerprint for the benzene ring.[10−12] The spectrum in Figure 4 shows that the unconnected carbons are gathered in a small energy interval, something that is predicted for other substituted benzenes with strong substituents as well[10,12] (the stronger the substituent the larger the shift for the connected carbon but the smaller the spread of the unconnected carbons, see Discussion in ref 12). The two, oxygen- and nitrogen-, connected benzene carbons show characteristic shifts of about 2 eV with respect to the other ring carbons; the actual energy shifts accord well with those predicted and observed in aniline and phenol.[13] The fourth feature, shifted as much as 3 eV from the first benzene-ring band, is due to the C1s−π^* transition for the carbon connected to the sulphur end. This unusually large shift must be attributed to the charge depletion of this carbon by its three nearest, N, O, and S neighbors.

Beyond 289 eV one finds a multiple structure due to onsets of the ionization edges, which here spans a large interval owing to the several chemically shifted carbons from MBO. Discrete transitions in addition to the π^* resonances are predicted but are comparatively weak and not significant for the analysis. We note here that for single-ring systems the STEX method

TABLE 2: Main STEX Excitation Energies (below the Ionization Thresholds) and Oscillator Strengths (in Parentheses) at the C, N, and O K-Edges and S L-Edge of MBO[a]

C K-edge	N K-edge	O K-edge	S L-edge
C_1	403.85 (0.013)	537.36 (0.011)	lower series ($2p_{3/2}$)
289.62 (0.038)	404.56 (0.003)	538.67 (0.002)	164.74 (0.003)
293.19 IP	405.35 (0.006)	538.89 (0.002)	164.79 (0.001)
C_2	405.46 (0.001)	539.15 (0.001)	165.68 (0.001)
287.72 (0.034)	406.24 (0.001)	540.58 IP	166.18 (0.001)
289.54 (0.002)	406.81 (0.001)		166.19 (0.001)
290.10 (0.003)	407.46 (0.002)		166.61 (0.001)
291.67 IP	407.01 IP		166.62 (0.001)
C_3			166.79 (0.001)
287.70 (0.036)			166.94 (0.001)
289.22 (0.002)			166.95 (0.001)
291.42 IP			167.13 (0.002)
C_4			167.14 (0.001)
287.67 (0.043)			167.54 (0.003)
289.20 (0.001)			167.94 IP
291.42 IP			upper series ($2p_{1/2}$)
C_5			165.94 (0.002)
287.54 (0.033)			165.99 (0.001)
289.18 (0.002)			
291.45 IP			
C_6			
289.26 (0.039)			
290.50 (0.003)			
293.01 IP			
C_7			
290.12 (0.063)			
294.25 (0.002)			
295.71 IP			

[a] For the C K-edge, the seven channels (C_1 to C_7) due to the seven inequivalent carbon atoms are included. For the S L-edge the two channels, due to the $2p_{3/2}$ and $2p_{1/2}$ core levels, are included. ΔSCF ionization thresholds (IP) are reported.

attributes a single strong π^* and a single strong σ^* resonance,[14] in some contradiction to what is obtained by multiple scattering calculation ($X_\alpha-MS$).[1]

For a better insight into the π^* region of the C K-edge we have carried out measurements in higher resolution conditions. The experimental spectrum obtained for $\vartheta = 15°$, together with a fit analysis in the 284−289 eV energy region, is shown in Figure 5, while in Table 3 are reported the relative data. As a main difference between experiment and theory we observe that four peaks identified from the deconvolution are not obtained by the calculation. Two of them can be related to the "a" transition and the other two to the "c" transition. The first two are respectively 0.38 and 0.80 eV shifted from the main peak in the feature "a", whereas the other two are at 0.28 and 0.56 eV from the main peak of the feature "c". Considering that the calculations are performed in the vertical transition approximation, i.e. at fixed positions of the nuclei, these transitions, appearing at a constant energy differences from the main peaks, may be tentatively interpreted as due to vibrational excitations. We observe that the NEXAFS π^* band in benzene shows shoulders of similar character,[15] and C−H vibrational energies of 0.5 eV have been predicted for the C1s−π^* state of that molecule.[16] Moreover, from the experimental C K-edge of Figure 5, it should be noted that transition "d" has a smaller width if compared with the other transitions (from "a" to "c") showing a quasitriangular shape deriving from the transmission function of the used monochromator. This fact could be due to different vibrational modes involved in the "d" transition, with respect to core excitations at the C_1 to C_6 atoms. The different

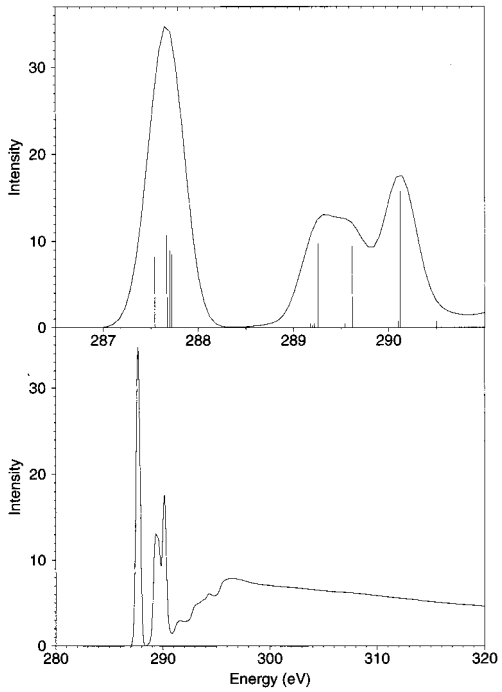

Figure 4. C K-edge spectrum calculated by the STEX method for MBO convoluted with a Gaussian function (fwhm = 0.40 eV) in the low-energy region. In the upper part the π^* region is highlighted together with the bar diagram describing the energy position and intensity of the transitions. The absorption cross section (full line) is given in Mb; the absolute values of the oscillator strengths (bars) are reported in Table 2.

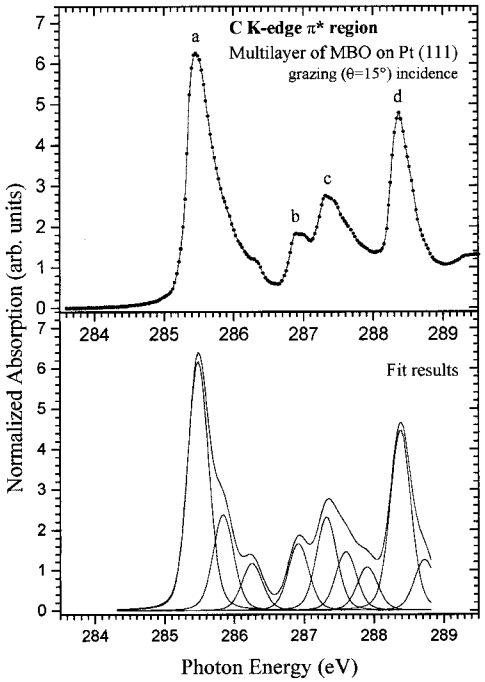

Figure 5. π^* region of the higher resolved experimental C K-edge spectrum of MBO obtained at grazing photon incidence angle with respect to the surface ($\vartheta = 15°$). Fitting results are included.

intensity ratio for the "b" and "c" transitions found in the experimental (Figure 5) and theoretical (Figure 4) spectra can also probably be ascribed to the presence of vibrational states non included in the theoretical model. Assuming, on the basis of the calculations, that the electronic transitions corresponding to the structures "b" and "c" have comparable intensity, the experimentally observed increased intensity of peak "c" with

TABLE 3: Fitting Results Obtained for the Experimental Higher Resolution π^* Region of the C K-Edge of Figure 5 and N K-Edge of Figure 8[a]

C K-edge	N K-edge
285.49 (6.08)	402.85 (4.70)
285.87 (2.13)	403.22 (0.89)
286.28 (1.05)	404.21 (1.56)
286.92 (1.61)	404.66 (1.00)
287.34 (2.31)	
287.60 (1.21)	
287.90 (1.01)	
288.40 (4.56)	
288.74 (1.22)	

[a] From the fit a width of 0.38 eV and 0.62 eV are obtained respectively for the C K-edge and N K-edge.

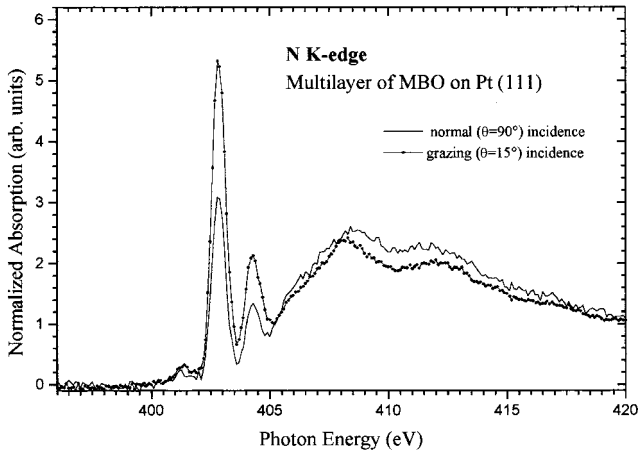

Figure 6. Experimental N K-edge spectra of MBO multilayer adsorbed on Pt(111) single crystal at 95 K, at grazing and normal photon incidence angle with respect to the surface.

respect to peak "b" could be due to the superposition, around 287.3 eV, of the second peak of the vibrational progression for excitation at C_6 with the first peak of the vibrational progression for excitation at C_1. A firmer confirmation of this hypothesis could be obtained by calculations on MBO that take into account explicitly vibrational states and Franck−Condon factors for the core-excited states. Such calculations will be the subject of a forthcoming investigation.

B. Nitrogen K-Edge. The experimental N K-edge spectra recorded for MBO multilayer on a Pt(111) surface (at 95 K) at grazing and normal incidence are reported in Figure 6. The N K-edge spectrum exhibits a lower number of transitions compared with the C K-edge spectrum, that is of course complicated by the presence in the molecule of various chemically shifted carbon atoms. Two main peaks are evident, respectively, at 402.8 and 404.3 eV, and two broader resonances are visible at 408.2 and 412.2 eV; the energy values are collected in Table 1.

Figure 7 reports the computed spectrum at the N K-edge, convoluted with a Gaussian function (fwhm = 0.60 eV). In the lower part of the figure the full spectrum, from 400 to 420 eV, is shown, while in the upper part the π^* region is highlighted together with the bar diagram describing the energy position and intensity of the transitions (also reported in Table 2). The arrow marks the opening of the ionization channel. For a better comparison between the calculation and the experimental spectrum, the low-energy π^* region has been measured at higher instrumental resolution; the spectrum obtained for $\vartheta = 15°$ is shown in Figure 8 together with the results of the deconvolution (the relative data are reported in Table 3).

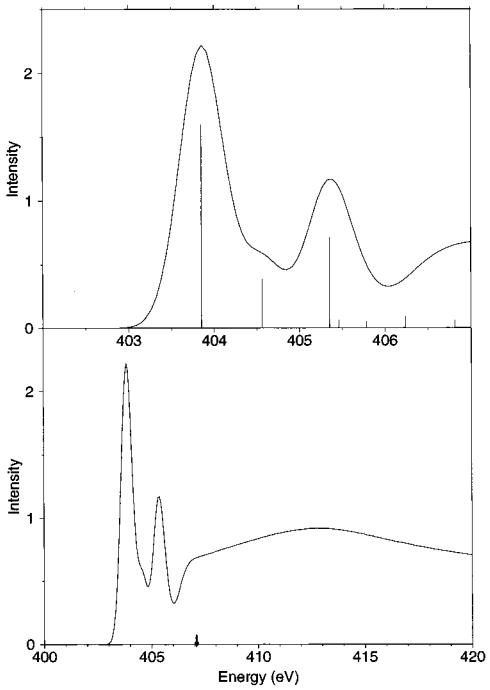

Figure 7. Calculated N K-edge spectra by the STEX method for MBO convoluted with a Gaussian function (fwhm = 0.60 eV) in the low-energy region. In the upper part the π^* region is highlighted together with the bar diagram describing the energy position and intensity of the transitions. The absorption cross section (full line) is given in Mb; the absolute values of the oscillator strengths (bars) are reported in Table 2. The arrow marks the position of the core ionization threshold.

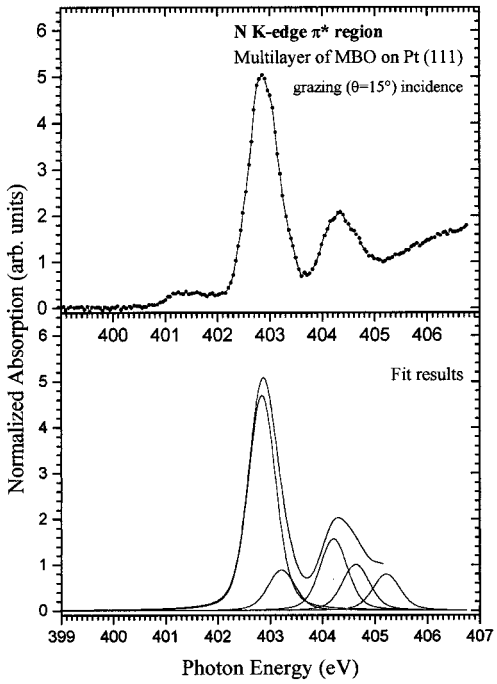

Figure 8. π^* region of the higher resolved experimental N K-edge spectrum of MBO obtained at grazing photon incidence angle with respect to the surface ($\vartheta = 15°$). Fitting results are included.

In the π^* region, the calculations predict three main discrete transitions at 403.8, 404.6, and 405.3 eV (with intensity 0.013, 0.003, and 0.006, respectively). Comparison between calculated and experimental higher resolved spectra show good agreement, except for the expected energy shift of the theoretical excitation energies. The first and third excitations are due to out-of-plane orbitals (both fairly compact); the second is due to an N−H σ^*

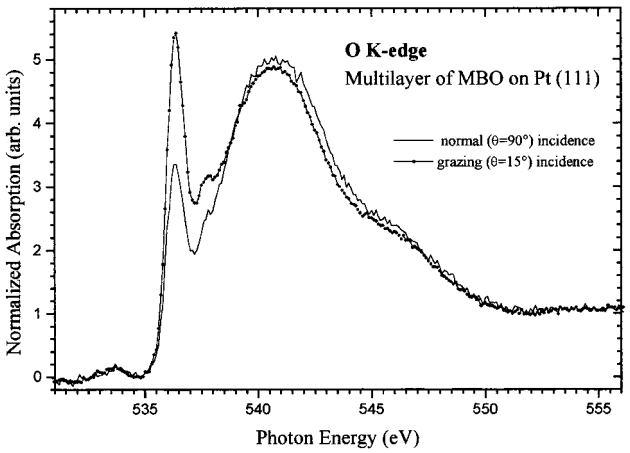

Figure 9. Experimental O K-edge spectra of MBO multilayer adsorbed on Pt(111) single crystal at 95 K, at grazing and normal photon incidence angle with respect to the surface.

level. The nitrogen spectrum is unusual because two π^* peaks appear in the discrete part. Despite that N is formally single bonded, it anyway provides a large discrete-to-continuum intensity ratio similar to that observed, for instance, in pyridine.[17] One can perhaps explain this by a "residual" conjugated character and by the presence of the fused benzene ring. The two N−C bond lengths in MBO are in fact 1.34 (N−C_7) and 1.41 (N−C_6)Å, which are values comparable to that in pyridine with a partial double bond, but considerably shorter than the typical length of a single N−C bond (1.48 Å). One accordingly finds a shape resonance quite far beyond the IP (≃7 eV).

C. Oxygen K-Edge. The experimental O K-edge spectra recorded for the MBO multilayer on the Pt(111) surface (at 95 K) at grazing and normal incidence are reported in Figure 9. As previously discussed for the N K-edge and for the same reasons, the O K-edge spectra exhibit a lower number of transitions compared with the C K-edge. Two main peaks are evident at 536.4 and 537.8 eV, and two broader resonances are visible at 540.7 and 546.2 eV; the energies of the transitions are collected in Table 1.

The STEX spectrum, convoluted with a Gaussian function (fwhm = 1.20 eV), is reported in Figure 10: the lower part contains the photoabsorption cross section from 530 to 560 eV, while in the upper part the π^* region is highlighted together with the bar diagram describing the energy position and intensity of the transitions (also reported in Table 2). The arrow marks the position of the core ionization threshold.

The computed O K-edge spectrum presents in the π^* region four intense transitions at 537.4, 538.7, 538.9, and 539.1 eV; their oscillator strengths are 0.011, 0.002, 0.002, and 0.001, respectively. The first excitation is in good agreement with the strong π^* peak observed experimentally at 536.4 eV, while the three transitions found in the theoretical spectrum around 539 eV correspond to the unique experimental peak around 537.8 eV. The very strong band beyond the edge, around 541 eV in Figure 9, is only partially accounted for by the calculations. That particularly strong structure is probably due also to the presence of multielectron excitations that cannot be described by the one-electron STEX technique. The comparison of calculated and experimental spectra shows anyway a satisfactory agreement also at the O K-edge. The low resolution of the experiment in this energy range does not allow to identify any vibrational structure.

D. Sulphur L-Edge. The experimental S L-edge spectra at grazing and normal photon incidence are reported in Figure 11.

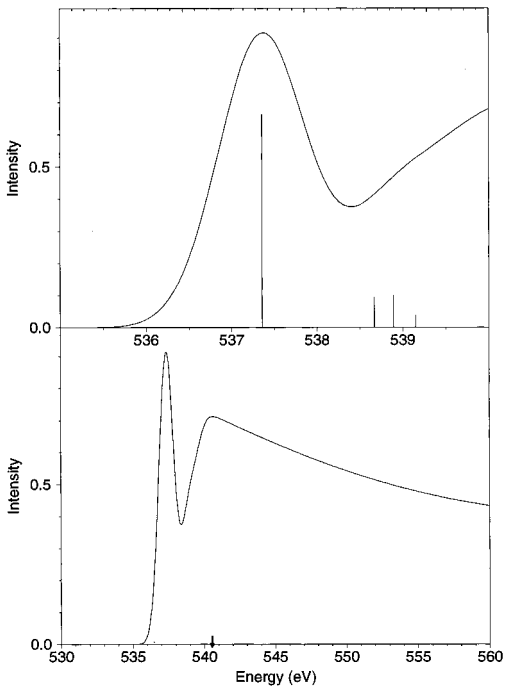

Figure 10. Calculated O K-edge spectra by the STEX method for MBO convoluted with a Gaussian function (fwhm = 1.20 eV) in the low-energy region. In the upper part the π^* region is highlighted together with the bar diagram describing the energy position and intensity of the transitions. The absorption cross section (full line) is given in Mb; the absolute values of the oscillator strengths (bars) are reported in Table 2. The arrow marks the position of the core ionization threshold.

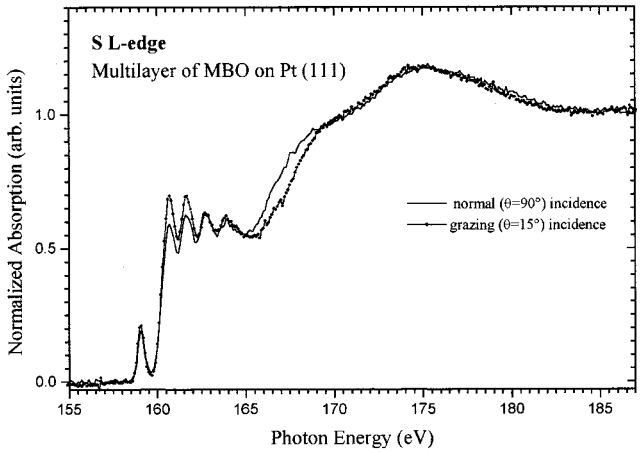

Figure 11. Experimental S L-edge spectra of MBO multilayer adsorbed on Pt(111) single crystal at 95 K, at grazing and normal photon incidence angle with respect to the surface.

In the lower energy side, narrow resonances at 159.1, 160.7, 161.7, 162.8, and 164.0 eV are observed, while broad resonances are visible at 169.5 eV (probably due to onsets of the ionization edges, see Table 1) and 174.6 eV.

The S L-edge computed spectrum, convoluted with a Gaussian function (fwhm = 0.60 eV) is reported in Figure 12; the full spectrum, from 160 to 195 eV, is shown in the lower part, while in the upper part the π^* region is highlighted together with the bar diagram describing energy position and intensity of the main transitions (also reported in Table 2). The arrows mark the position of the core ionization thresholds for the $S2p_{3/2}$ (lower) and the $S2p_{1/2}$ (upper) channel.

The theoretical analysis of the sulphur spectrum is complicated due to several reasons: the spin−orbit splitting produces

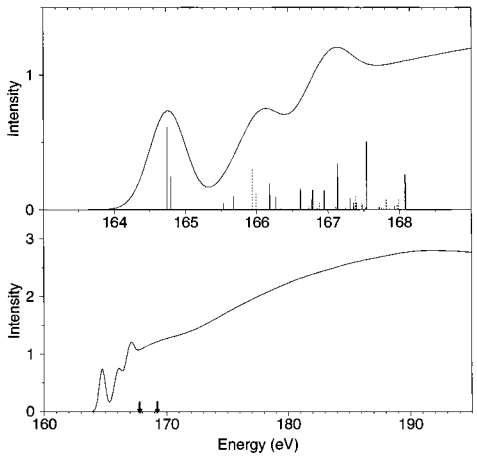

Figure 12. Calculated S L-edge spectra by the STEX method for MBO convoluted with a Gaussian function (fwhm = 0.40 eV) in the low-energy region. In the upper part the π^* region is highlighted together with the bar diagram describing the energy position and intensity of the transitions. The absorption cross section (full line) is given in Mb; the absolute values of the oscillator strengths (bars) are reported in Table 2. The arrow marks the positions of the core ionization thresholds.

a duplication of the spectrum, and the 2p level is molecular field splitted into quasidegenerate sublevels with special implications for the static exchange analysis. The presence of the spin−orbit splitting is often accounted for by superposing two spectra shifted by the experimental (here $S2p_{3/2,1/2}$) spin−orbit splitting, and assuming a statistical value (here 2 to 1) for the corresponding intensities. Molecular field splitting of the core (here 2p) level implicates intermediate coupling for intensities and the appearance of "new" fine structure levels in high resolution NEXAFS of small species.[18,19] Of more serious concern for the STEX analysis of MBO is, however, the coupling of excitations from quasi-degenerate molecular orbitals corresponding to the 2p level. This kind of channel interaction is neglected in the static-exchange independent channel approximation here adopted. STEX is in fact mainly designed for the representation of core excitation at the K-edge where the excitation channels are decoupled because of energy or spatial separation of the core orbitals involved.

The experimental spectrum shows a low ratio of discrete to continuum intensity with basically three strong resonance peaks followed by a weaker Rydberg series, and multielectron excitations superimposed on a shape resonance structure close to the continuum. In order to take into account the experimental splitting value of 1.2 eV, obtained from photoemission,[20,21] the $2p_{3/2}(L_3)$ channel spectrum has been obtained from the non-relativistic results by subtracting $(^1/_3)(1.2)$ eV from the calculated IP, while for the $2p_{1/2}(L_2)$ channel spectrum $(^2/_3)(1.2)$ eV has been added. The calculated spectra from the two separate channels were then added to give the total spectrum. The first peak in the total NEXAFS spectrum is solely due to excitations from the $2p_{3/2}$ channel, while the remaining structures are due to a mixture of excitations from both channels (see Table 2). The theoretical spectrum as a whole looks like the experimental one but fails in reproducing details of the structures below the threshold. This could probably be ascribed to the approximations of the theoretical model previously discussed, mainly the neglect of the excitation channel coupling that could be relevant at the L-edge. On the other hand, recent calculations for the S L-edge of OCS[19] have shown a quite good agreement with the experiment. Further applications to different sulphur containing molecules will probably help to establish the applicability of the STEX independent channel model to the simulation of NEXAFS spectra at the L-edge. The values of the IP's (168.49 eV for 2p along the bond, 168.34 eV for 2p orthogonal to the bond) computed by the ΔSCF procedure, give a molecular field splitting in MBO very close to that measured in OCS.[22] When the experimental spin-orbit splitting of 1.2 eV is employed to correct the nonrelativistic results, a satisfactory agreement is also obtained between theory IP[S-$2p_{3/2}$] = 167.9/168.1 eV and experiment IP[S-$2p_{3/2}$] = 167.9 eV.[23] It can be observed that the chemical shift for the IP at the S L-edge is negative and quite strong when compared to the values of IP[S-$2p_{3/2}$] of similar molecules (CS_2 = 169.8 eV[24] and OCS = 170.72 eV[25]). The large chemical shift for the S L-edge IP of MBO may be considered as an indication of the peculiar electronic structure of the five-member ring of this molecule. This is also evident in the unusually high value of the core IP of the carbon atom (C_7) bond to sulphur.

E. Angular Distributions. A strong variation in intensity of the low energy resonances in the experimental C, N, and O K-edges spectra (see Figures 2, 6, and 9) is observed going from grazing to normal incidence of the photons with respect to the platinum surface. This is a clear indication of an average orientation of the molecules on the surface. Assuming that the molecule maintains its planarity after adsorption, the angle between the MBO molecular plane and the Pt(111) surface can be calculated from the ratio of the area of the π^* peaks at the two photon incidence angles. Considering that the multilayer has been obtained by deposition of MBO molecules on a surface with high rotational symmetry, we applied the following formula for the intensity of the π^* peaks, where the dependence from the azimuthal angle is averaged out[1]

$$I_{\pi^*} \propto P\,{}^1/_3[1 + {}^1/_2(3\cos^2\vartheta - 1)\,(3\cos^2\alpha - 1)] + (1 - P)\,{}^1/_2\sin^2\alpha \quad (1)$$

where P is the photon polarization factor in the plane of the electron beam orbit of the storage ring (equal to 0.85 in the present case), ϑ is the X-ray incidence angle from the surface, and α is the angle between the direction of the π^* molecular orbital and the normal to the Pt(111) surface.

The peak area ratio obtained for the π^* resonance at 285.5 eV in the C K-edge spectra (grazing to normal) is 1.46, indicating that the benzene ring plane of the MBO molecules in the multilayer on Pt(111) tilts about 48° with respect to the surface. Very similar peak area ratios, 1.73 and 1.59, obtained from the π^* resonance at 402.8 and 536.4 eV in the N and O K-edge spectra, respectively, confirm a tilt angle around 48° and that the MBO molecule remains planar when adsorbed as a multilayer phase on Pt(111) at 95 K. Previous NEXAFS experiments[5] on MBO multilayer on Pt(111) showed a similar angular dependence of the π^* resonance intensities but the tilt angle deduced was different. This can be ascribed to the different thickness of the MBO layer obtained in the two experiments. In fact, other NEXAFS measurements on MBO adsorbed at 95 K on Pt(111) show that there is a dependence of the MBO molecular plane orientation as a function of the layer thickness.[23]

As discussed above, the S L-edge spectrum of the multilayer exhibits features quite different from those of the C, N, and O K-edge spectra; in particular, it does not show intense π^* resonances and no strong polarization dependence is observed. This can be ascribed to the different dipole selection rules acting at the L-edge, i.e., to the fact that excitations at the S L-edge are dominated by atomic p → d contributions and the spectrum is given by the sum of the photo absorption intensities of three

almost degenerate channels. Because the orbitals that are excited ($2p_x$, $2p_y$, and $2p_z$) point to orthogonal directions, we will have, for different directions of the photon beam, different contributions to the three separate channel intensities, but essentially the same superposition of the three, leading to an almost angular independent total intensity.

V. Conclusions

This paper reports a full comparison between experimental and calculated NEXAFS spectra of 2-mercaptobenzoxazole in a condensed multilayer on platinum. It is an unusual investigation in that the NEXAFS spectra have been experimentally collected and theoretically simulated at four different edges for the same molecule. The good general agreement between experiment and theory allowed a detailed discussion and attribution of the various features of the spectra. In particular, it was possible to deduce that the MBO molecules in the multilayer sample are strongly oriented with a tilt angle of about 48°. Vibrational contributions have also been tentatively identified in the highly resolved C K-edge experimental spectra and will be the subject of future theoretical investigations of MBO and of other organic molecules.

Acknowledgment. The Authors thank people from the SACEMOR beam line at Super-Aco (LURE) (Dr. Ph. Parent and Dr. C. Laffon) for their very useful helps during the measurements and for helpful discussions.

References and Notes

(1) Stöhr, J. *NEXAFS Spectroscopy*; Springer Verlag: Berlin, 1992.
(2) Johnson, A. L.; Muetterties, E. L.; Stöhr, J.; Sette, F. *J. Phys. Chem.* **1985**, *89*, 4071.
(3) Ågren, H.; Carravetta, V.; Vahtras, O.; Pettersson, L. G. M. *Chem. Phys. Lett.* **1994**, *222*, 75.
(4) Ågren, H.; Carravetta, V.; Vahtras, O.; Pettersson, L. G. M. *Theor. Chem. Acc.* **1997**, *97*, 14.
(5) Contini, G.; Ciccioli, A.; Laffon, C.; Parent, Ph.; Polzonetti, G. *Surf. Sci.* **1998**, *412/413*, 158.
(6) Dunning, T. H., Jr. *J. Chem. Phys.* **1971**, *55*, 716.
(7) Sadlej, A. J. *Coll. Czech. Chem. Commun.* **1988**, *53*, 1995.
(8) Groth, P. *Acta Chem. Scand.* **1973**, *27*, 945.
(9) Langhoff, P. W. In *Theory and Application of Moment Methods in Many-Fermion Systems*; Dalton, B. J., Grimes, S. M., Vary, J. P., Williams, S. A., Eds. Plenum: New York, 1980; p 191.
(10) Pettersson, L. G. M.; Ågren, H.; Schürmann, B. L.; Lippitz, A.; Unger, W. E. S. *Int. J. Quantum Chem.* **1997**, *63*, 749.
(11) Carravetta, V.; Polzonetti, G.; Iucci, G.; Russo, M. V.; Paolucci, G.; Barnaba, M. *Chem. Phys. Lett.* **1998**, *288*, 37.
(12) Plachkevytch, O.; Yang, L.; Vahtras, O.; Ågren, H.; Pettersson, L. G. M. *Chem. Phys.* **1997**, *222*, 125.
(13) Yang, L.; Plashkevych, O.; Ågren, Hans; Pettersson, L. G. M. *J. Phys. IV* **1997**, *7*, 227.
(14) Ågren, H.; Carravetta, V.; Vahtras, O. *Chem. Phys.* **1995**, *196*, 47.
(15) Ma, Y.; Sette, F.; Meigs, G.; Modesti, S.; Chen, C. T. *Phys. Rev. Lett.* **1989**, *63*, 2044.
(16) Norman, P.; Agren, Hans *J. Mol. Struct. (THEOCHEM)* **1997**, *401*, 107.
(17) Horsley, J. A.; Stöhr, J.; Hitchcock, A. P.; Newbury, D. G.; Johnson, A. L.; Sette, F. *J. Chem. Phys.* **1985**, *83*, 6099.
(18) Fink, R. F.; Kivilompolo, M.; Aksela, H.; Aksela, S. *Phys. Rev. A* **1998**, *58*, 988.
(19) Magnuson, M.; Guo, J. H.; Såthe, C.; Glans, P.; Rubensson, J. E.; Nordgren, J.; Yang, L.; Sałek, P.; Ågren, H. 1998. Manuscript to be published.
(20) Wight, G. R.; Brion, C. E. *J. Electron Spectrosc. Relat. Phenom.* **1974**, *4*, 25.
(21) Contini, G.; Di Castro, V.; Polzonetti, G.; Comelli, G.; Brena, B.; Marabini, A. M. *Surf. Sci.* **1997**, *65*, 391.
(22) Siggel, M. R. F.; Field, C.; Saethre, L. J.; Børve, K. J.; Thomas, T. D. *J. Chem. Phys.* **1996**, *105*, 9035.
(23) Contini, G. et al. Manuscript in preparation.
(24) Siegbahn, K.; Nordling, C.; Johansson, G.; Hedman, J.; Hedén, P. F.; Hamrin, K.; Gelius, U.; Bergmark, T.; Werme, L. O.; Manne, R.; Baer, Y. *Esca Applied to Free Molecules*; North-Holland Publishing Company: Amsterdam, 1969.
(25) Brems, V.; Nestmann, B. M.; Peyerimhoff, S. D. *Chem. Phys. Lett.* **1998**, *287*, 255.